INTERNATIONAL JOURNAL FOR NUMERICAL AND ANALYTICAL METHODS IN GEOMECHANICS, VOL. 20, 753–767 (1996)

INVESTIGATION OF IMPACT STRESSES INDUCED IN LABORATORY DYNAMIC COMPACTION OF SOFT SOILS

H. S. THILAKASIRI, M. GUNARATNE, G. MULLINS, P. STINNETTE AND B. JORY†

Department of Civil and Environmental Engineering, University of South Florida, Tampa, FL 33647, U.S.A.

SUMMARY

The majority of currently available analytical tools to predict ground stresses due to impact are based on linear spring-dashpot dynamic models. Although these simple models adequately represent stiff ground possessing linear visco-elastic behaviour, they suffer from two striking limitations when applied to relatively softer ground; (1) the inability to account for the permanent deformation resulting from impact, (2) failure to incorporate stiffness changes of softer soil within the impact duration. In this paper, the authors present an improved analytical approach formulated on the basis of a series of laboratory impact tests, to address the shortcomings of the current dynamic models in relation to soft soils. In this procedure, the impact zone is modelled as three distinct zones; (1) a zone beneath the falling weight undergoing non-linear axial deformation while being in vertical motion, (2) an inner zone immediately surrounding zone 1 with non-linear shear deformation, and (3) an outer zone undergoing a relatively lower degree of (linear) shear deformation. The soil constitutive parameters pertinent to the model are obtained from a modified dynamic compression test that simulates the impact conditions. It is shown that analytical predictions of the impact stress history and penetration are in agreement with test results. The findings are useful in the exploration of dynamic compaction techniques that will be effective in soft soil improvement.

KEY WORDS: dynamic; compaction; soil; damping; non-linear stressing

1. INTRODUCTION

A number of analytical models have been proposed by several researchers[1–4] in recent years to estimate surface stresses during dynamic compaction. In these models, it is assumed that the soil behaviour is linear elastic, isotropic and hence can be modelled by a linear spring and a linear dashpot. However, it is a common observation made during dynamic compaction of soft soil that the soil mass close to the surface is subjected to a very high strain level resulting in permanent deformation. Obviously a model that employs a linear spring and a linear dashpot is unable to simulate these observations because non-linearity is clearly exhibited by soils at high strain levels. Apart from the above-mentioned simplified models, Chow *et al.*[3] proposed a different analytical approach where the one-dimensional wave equation model for pile-driving analysis is modified by replacing the pile with a soil column extending to at least the anticipated depth of improvement. In this method, the soil surrounding the soil column is represented by linear elastic springs and linear dashpots. Furthermore, they adopted an implicit finite element method to solve the equation of motion of the soil column.

†Present address: Florida Department of transportation, Bartow, FL, U.S.A.

CCC 0363–9061/96/100753–15

Received 9 September 1994
Revised 12 January 1996

An improved analytical model is proposed in this paper to estimate the surface stress and the surface deformation, accounting for non-linearity of soil immediately below the drop hammer as well as that of the immediate neighbourhood of the hammer. In this procedure, equations of motion are separately written for three zones distinguished by their mode and degree of deformation while satisfying compatibility. A numerical procedure is adopted to solve these equations of motion because of complexity arising from the constitutive model that accounts for non-linearity. The solution procedure uses an explicit direct time integration together with lumped mass formulation for computational efficiency. Finally, analytical predictions of the impact surface stress history and penetration are compared with laboratory measurements.

2. EXPERIMENTAL OBSERVATIONS

Figure 1 shows a typical plot of the impact surface stress history recorded during the authors' experiments on a wet organic soil by employing a falling hammer instrumented with sensitive pressure transducers. The sensitivity of the data acquisition system is discussed in the ensuing Section 4 on the experimental set-up. The stress–time plot such as that shown in Figure 1 obtained from a series of tests consistently demonstrate the existence of two distinct regions:

(1) An immediate peak followed by rapidly diminishing stress. This phase of the stress history usually lasts only an extremely small time (1–2 ms) thus possibly eluding detection without a sensitive data acquisition system. This could be one reason why such an instantaneous peak has not been documented in previous experimental studies.
(2) A subsequent oscillatory stress pattern. This phase of the stress pulse on the other hand has been the subject of most previous experimental and analytical investigations.

3. MATHEMATICAL IDEALIZATION

From the perspective of deformation, the soil mass in the impact vicinity can be considered as being comprised of three distinct zones (Figure 2):

Zone 1: soil under the falling hammer in the zone of influence undergoing significant vertical deformation that permits it to be considered as a moving or participating soil mass,
Zone 2: soil in the immediate neighbourhood undergoing excessive shear deformations that can only be characterized by non-linear models,

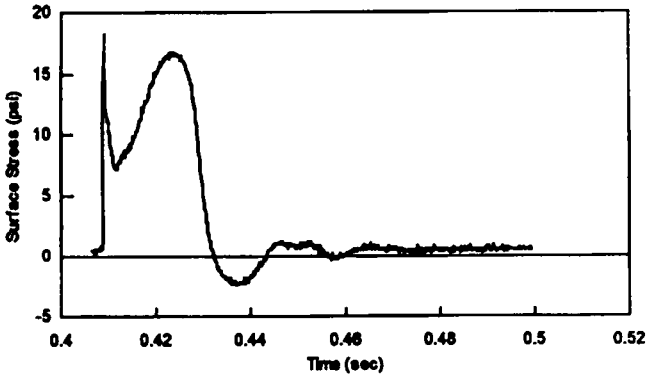

Figure 1. Typical experimental impact stress history

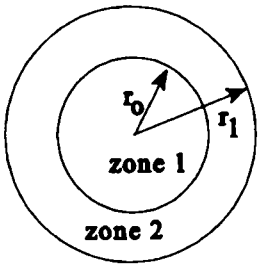

Figure 2. Plan view of the impact vicinity

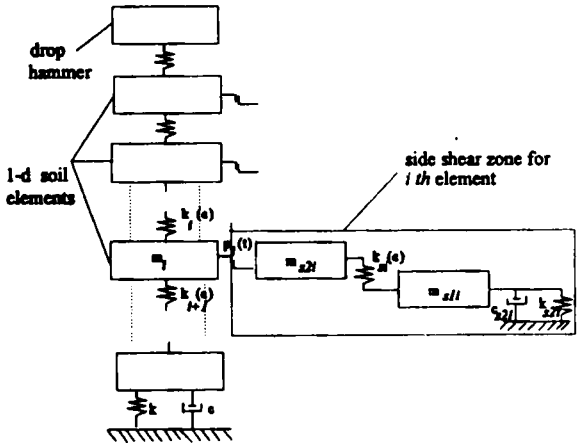

Figure 3. Dynamic model (shear zone is shown only for the ith element)

Zone 3: soil in the outer region undergoing limited shear deformations within linear elastic limits.

The authors' analytical formulation discussed here is founded on consideration of the mechanics of these three zones. The analytical formulation is kept simple by replacing the soil in the above zones with equivalent lumped masses. Researchers have observed that the depth of the zone of influence (z) during dynamic compaction varies in the range of $\sqrt{(W_1 h)} \geqslant z \geqslant 1/2\sqrt{W_1 h)}$,[6,7] where W_1 and h are drop weight in tonnes and drop height in meters, respectively. Hence, in their formulations the authors suggest that the vertical depth (z) of the above non-linear zones should at least extend to a depth of $\sqrt{(W_1 h)}$. In the mathematical discretization, zones 1 and 2 up to the depth of influence are divided into elements of equal thickness as shown in Figure 3. Since the vertical strain within each element is assumed to be uniform, their thickness should be decided by a sensitivity analysis.

Since the strains in zone 1 are large, it is logical to expect non-linear behaviour. Thus, the soil elements in that zone are replaced in the current model by moving solid lumped masses (m_i) having the same cross-sectional area as that of the drop weight and are connected by non-linear

springs of stiffness $k_i(\varepsilon)$ as shown in Figure 3. $k_i(\varepsilon)$ can be expressed by $M_i(\varepsilon)A/L$ where $M_i(\varepsilon)$, A and L are the constrained modulus corresponding to the current strain (ε) (Section 3.1), cross-sectional area of the element and the current length of the element, respectively. The soil half-space beneath the immediate vicinity of the non-linear soil column is modelled by a linear spring (k) and a linear dashpot in parallel having a spring stiffness of $4G_s r_0/(1-\nu)$ and a dashpot coefficient of $3{\cdot}4Gr_0^2/(1-\nu)$ as proposed by Lysmer and Richart[8] in which r_0, G and ν are the radius of the soil column, initial shear modulus and the Poisson ratio, respectively. In the case where there is a stiff layer present within the zone of influence, the displacement of the last element is set to zero to account for it. In such a situation, the spring and the dashpot are not required.

On the other hand, the elements in annular zone 2, represented by two masses (m_{s1i} and m_{s2i}) of radius (r_1) surrounding zone 1 are also subjected to high strain levels. Therefore, its effect on the impact zone must also be modelled by non-linear shear stiffness properties (k_{si}). In this regard, the stiffness expression developed by El Naggar and Novak[9] would be appropriate. The expression for k_{si} is derived in the Appendix. The mass of the ith element in zone 2 is equally distributed to lumped masses m_{s1i} and m_{s2i} as shown in Figure 3. The elements in zone 2 interact with the corresponding elements in zone 1 through rigid plastic sliders $p_i(t)$ as shown in Figure 3.

Outside zone 2, the shear strains are small enough to permit the application of linear elastic constitutive relations. Thus, the shearing resistance of zone 3 is simulated by a linear spring (k_{s2i}) and a dashpot (c_{s2i}) having a stiffness of $2{\cdot}75G_s\,dz_i$ and a damping constant of $2\pi r_1\sqrt{\rho_s G_s}\,dz_i$, respectively, as proposed by Novak et al.[10] in which G_s, ρ_s and dz_i are the initial shear modulus, initial density and vertical thickness of elements in zone 2, respectively. Hence, zone 3 provides shear resistance to the vertical movement of elements in zone 2 through the parallel combination of spring k_{s2i} and c_{s2i}.

It is assumed that slipping can occur at the interface between the deforming soil elements in zone 1 and the elements in the surrounding zone 2 when the shear stress in the rigid plastic sliders $p_i(t)$ exceeds the maximum static resistance which is taken to be $k_0\sigma'_v \tan\Phi$; where, k_0, σ'_v and ϕ are coefficient of lateral earth pressure at rest, current vertical effective stress and angle of internal friction of the soil, respectively. It is accepted that the coefficient of lateral earth pressure depends on the over consolidation ratio (OCR) of the soil. Hence, in the proposed model k_0 is taken to be equal to $(1-\sin\phi)\sqrt{(\text{OCR})}$. Except for fully saturated low permeable soils with multiple impacts, the generation of pore water pressure in zone 1 is comparatively small[6] resulting in increased vertical effective stress in zone 1 during an impact. Therefore, it is important to note here that the maximum shear resistance changes during an impact even for a normally consolidated soil as the effective vertical stress changes with deformation of the soil column.

Finally, Newmark's explicit time step integration is employed to solve the equations of motion of the soil elements. The impacting hammer is disconnected from the numerical solution when the contact stress becomes less than zero.

If the depth of the non-linear zone is insignificant such as in the case of a small amplitude vibration, it is clear that the present model approaches the already accepted visco-elastic models, in which linear spring and a dashpot are in parallel (Figure 3). Further, the thickness of the influence zone can decrease with decrease in the drop weight and the drop height according to the aforementioned effective zone criterion ($\sqrt{Wh}$).

3.1. Determination of non-linear stiffness values

Figure 4 shows a typical axial stress–strain curve obtained for loading and unloading during a dynamic impact. The experimental procedure used to obtain Figure 4 is highlighted in Section 4. A unique feature of the stress–strain curve is a distinct yielding stage as shown in Figure 4 after

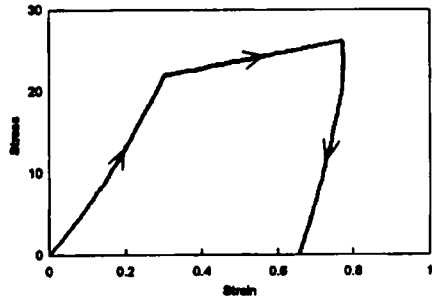

Figure 4. Experimental stress–strain curve

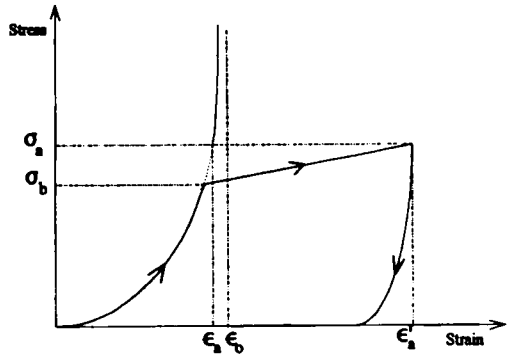

Figure 5. Typical theoretical stress–strain graph with symbols used in mathematical expressions

which a major portion of the axial strain is irrecoverable. This sudden change of the stiffness can be attributed to plastic flow resulting from shear failure. It was found that the pre-bearing capacity region of the curve can be conveniently expressed by the mathematical expression given by Ginsberg[11] for one-dimensional dynamic loading (equations (1) and (2)). Moreover, Ginsberg's[11] expression for the unloading phase correctly represented the unloading curve obtained by the authors as well (equations (5)–(6)). However, it should be noted that the post bearing capacity failure portion of the curve is linear with a small slope instead of being flat, indicating some strain hardening. Hence, based on Figure 4, the axial force in zone 1 can be determined by employing a constitutive relationship similar to that proposed by Ginsburg[11] for non-linear uniaxial dynamic compression. During each time step, the incremental strain in a given element is calculated based on the shortening of the element during the period and the current length of the element. Then, those incremental strains are summed up to estimate the total strain in the element and the corresponding axial stress from Figure 4. While the shape of the stress–strain curve proposed for loading and unloading is shown in Figure 5, the related mathematical relationships modified from the original Ginsburg model to include plastic flow, are expressed below.

For the loading stage
Up to the bearing capacity

$$\sigma = \frac{M_0 \varepsilon \varepsilon_0}{\{\varepsilon_0 - \varepsilon\}} \tag{1}$$

$$M(\varepsilon) = \frac{M_0 \varepsilon_0^2}{\{\varepsilon_0 - \varepsilon\}^2} \tag{2}$$

Beyond the bearing capacity

$$\sigma = k\{\varepsilon - \varepsilon_b\} + \sigma_b \tag{3}$$

$$M(\varepsilon) = k \tag{4}$$

For the unloading state

$$\sigma = M_0 \varepsilon_* \varepsilon_0 / \{\varepsilon_0 - \varepsilon_*\} \tag{5}$$

$$\varepsilon_* = (\varepsilon - (\varepsilon_a' - \varepsilon_a) - \varepsilon_a \eta / 1 - \eta \tag{6}$$

$$M(\varepsilon) = M_0 \varepsilon_0^2 / \{1 - \eta\}\{\varepsilon_0 - \varepsilon_*\}^2 \tag{7}$$

$$\varepsilon_a = \varepsilon_0 \sigma_a / (\sigma_a + M_0 \varepsilon_0) \tag{8}$$

where
M_0 = initial constrained modulus,
$M(\varepsilon)$ = constrained modulus at strain ε,
ε_0 = asymptotic value of strain corresponding to the pre-bearing failure portion,
η = a material constant,
ε_a' = strain at the beginning of the unloading phase,
σ_a = stress at the beginning of the unloading phase,
σ_b = bearing capacity,
k = modulus after the bearing capacity failure.

As mentioned in the mathematical idealization, the following expression for stiffness developed by El Naggar and Novak[9] assuming a plane strain condition are used for zone 2.

For loading

$$k_{s/i} = \frac{2\pi G_s}{\ln \dfrac{r_1/r_2 - \eta_0}{1 - \eta_0}} \tag{9}$$

For unloading

$$k_{s/i} = \frac{2\pi G_s}{\ln(r_1/r_0)} \tag{10}$$

where
r_1 = outer radius of the inner zone,
r_0 = radius of the soil column,
G_s = initial shear modulus,
τ_0 = shear stress at the axial element and shear element interface,
τ_f = ultimate shear strength,
$\eta_0 = \tau_0/\tau_f$.

3.2. Kinematic equations of the system

Using the notation indicated in Figure 6, the following equations of motion can be written for various components of the system:

For the drop hammer

$$w_1 - q_1(t) = \frac{w_1}{g} d_1''(t) \tag{11}$$

For the ith axial element (in Figure 6)

$$q_i(t) - q_{i+1}(t) - p_i(t) = m_i d_i''(t) \tag{12}$$

For ith shear element (in Figure 6)

$$p_i(t) - q_{si}(t) = m_{s1i} d_{s1i}''(t) \tag{13}$$

$$q_{si}(t) - k_{s2i} d_{s2i}(t) - c_{s2i} d_{s2i}'(t) = m_{s2i} d_{s2i}''(t) \tag{14}$$

where

$$k_{s2i} = 2{\cdot}75 G_s \, \mathrm{d}z_i, \tag{15}$$

$$c_{s2i} = 2\pi r_1 \sqrt{(\rho_s G_s)} \, \mathrm{d}z_i, \tag{16}$$

$\mathrm{d}z_i$ = thickness of the ith element in zone 2.

Newmark's explicit time step integration can be used to solve the equations (11)–(14) in combination with equations (17) and (18) as previously mentioned. For an element with a displacement $d(t)$ at any time t, Newmark's classical explicit time step integration algorithm (14) involves following recurrence relationships:

$$d_{n+1}(t) = d_n(t - \Delta t) + \Delta t \, d_n'(t - \Delta t) + \frac{\Delta t^2}{2} d_n''(t - \Delta t) \tag{17}$$

$$d_{n+1}'(t) = d_n'(t - \Delta t) + \Delta t(1 - \beta_1) d_n''(t - \Delta t) + \Delta t \beta_1 d_{n+1}''(t) \tag{18}$$

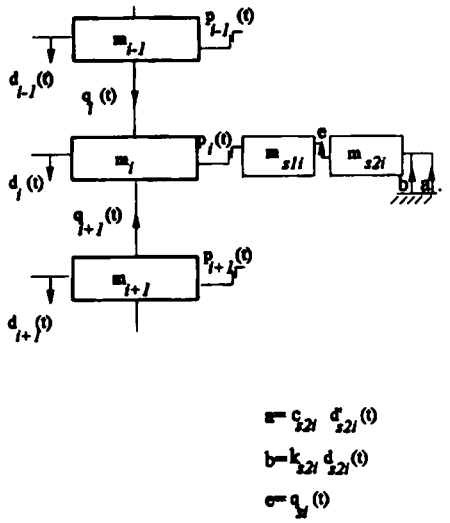

Figure 6. Free body diagrams for the ith axial and shear elements

where β_1 is Newmark's parameter, the value of which can be chosen for effective implementation of the particular algorithm.

Equation (17) can be used to explicitly obtain the current displacement $d_{n+1}(t)$ knowing the displacement, velocity and the acceleration of the element during the previous time step, while equation (18) enables one to express the current velocity of the element in terms of the current acceleration.

Thus, when equations (17) and (18) are separately applied to the elements in motion in Figure 3, it will facilitate the solution of equations (11)–(14) by evaluating the current displacement and the acceleration of each element based on the state of motion of the entire system at the preceding time step. Furthermore, at the end of each time step, element thicknesses and soil properties are upgraded according to the current strains, using the non-linear constitutive model described in the previous section. By repeating this procedure for a number of time steps, the numerical solution procedure can be successfully implemented. The explicit direct time integration algorithm is conditionally stable and the stability is governed by the magnitude of the time step size. It is found from the literature that the maximum size of the time step for a stable solution is related to the time required for an elastic wave to propagate across the shortest element of the mesh. In contrast to implicit algorithms, explicit algorithms require a large number of small time steps to avoid the solution of a large matrix equation which is typical of implicit methods at each time step.

4. EXPERIMENTAL SET-UP

The experimental set-up shown in Figure 7 was used to determine the dynamic impact stress due to a drop weight and the related stress–strain behaviour of an organic soil in the laboratory. The organic soil had a water content of 378 per cent, a we density of 1064 kg/m^3 (66 pcf) and an

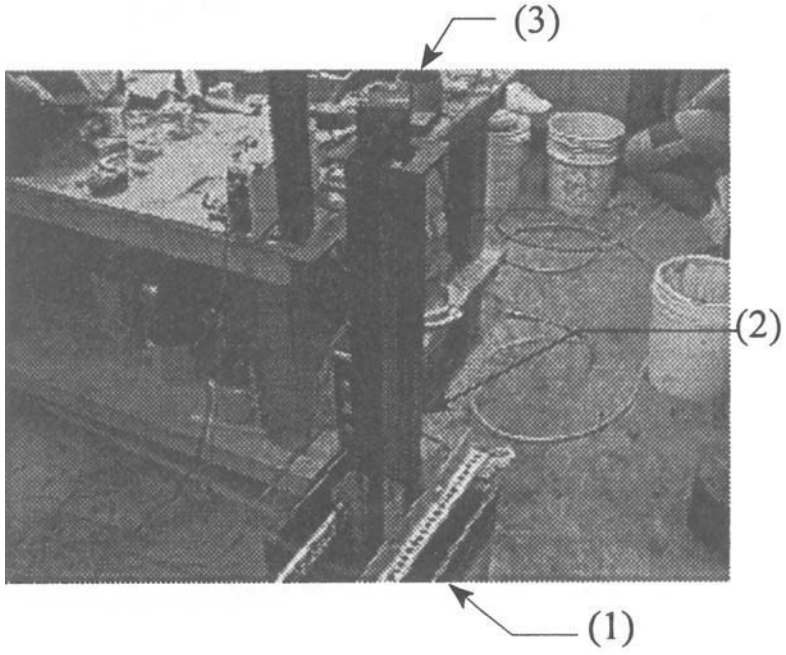

Figure 7. Experimental set-up

organic content of 80 per cent. The soil was compacted in a PVC lined 0·03 m^3 (one cubic foot-1′ × 1′ × 1′) container to a final bed depth of 10·16 cm (4 in) for the test used to get the surface stress history while a reduced depth of 2·6cm (1 in) was used for the test to determine the stress–strain relationship. A 0·923 m (3 ft) tall guide rail system (2) was placed on top of the box. A 2·27 kg (5 lb) steel weight with a 7·62 cm (3 in) square base (3) was held by an electro-magnet at the top of the guide rail. The weight was instrumented with five pressure transducers that were installed in such a manner that they were flush with the surface of the bottom of the weight. An accelerometer was also attached to the top of the weight so that its position was in line with the centre of gravity of the weight. The pressure transducers and the accelerometer were interfaced to a 486-33 MHz microcomputer through the use of a AT-MIO-16F-5 interface board.

Programs are written in Visual Basic to facilitate multiple channel data acquisition. A remote relay was used to simultaneously release the weight from the electro-mangnet and initiate data acquisition. The impact stress was sampled at a rate 10 000 samples/s for each of the five

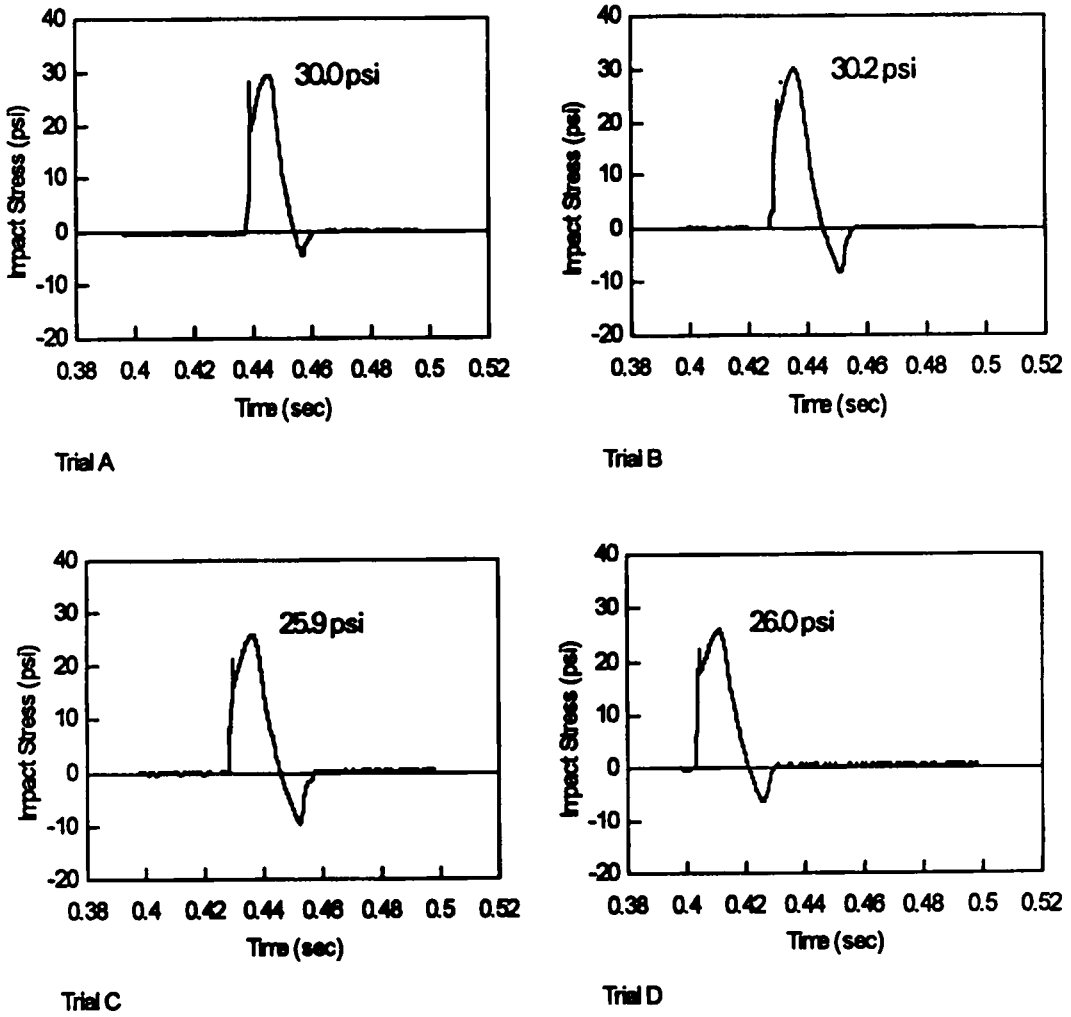

Figure 8. Impact stress versus time graphs for trials A–D

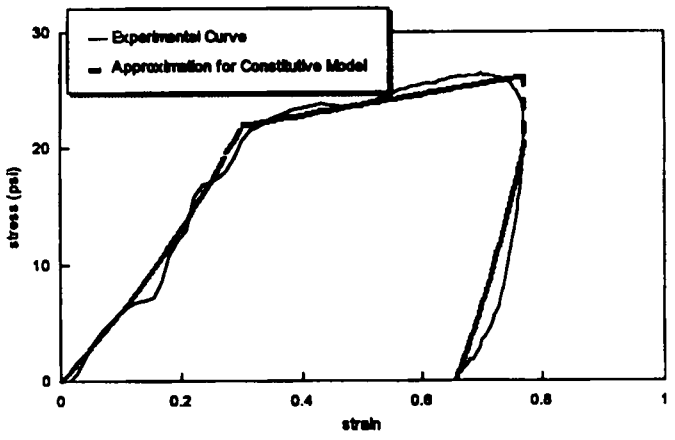

Figure 9. Experimental and simulated stress–strain curves

Table I. Model parameters for organic soil

Parameter	Assigned value
Outer radius of zone 2 (r_1)	8·56 cm ($2r_0$)
Initial modulus (M_0)	379 572 N/m^2
Poisson ratio	0·37
Angle of internal friction	35°
ε_0 (equations (1)–(8))	1·25
η (equations (6) and (7))	0·06
$K_0 = (1 - \sin\Phi)\sqrt{(\text{OCR})}$	0·4264
k (equations (3) and (4))	7·0 N/m^2

transducer channels in order to register the initial stress peak. Acceleration data was also sampled at a rate of 10 000 samples/s. Once data had been acquired and stored on the computer, data analysis was performed using LOTUS-123.

In order to verify reproduceability, four separate trials (A–D) were conducted using the same experimental set-up described above. Figure 8 shows the resulting impact stress versus time plot for each trial and the magnitude of the peak average impact stress. As seen from Figure 8, the peak average impact stress as well as the duration of impact are in agreement for all the trials.

By employing the accelerometer readings, the authors used the same test set-up with a thin soil layer to establish a non-linear stress–strain relationship for soil in zone 1 in the following manner. The vertical strain history can be deduced by converting the accelerometer results to displacements and then to corresponding strains assuming uniform strain throughout the thin layer of soil (2.5 cm) used in that test. Then, by comparing the average stress and strain histories at different stages of time in the soil layer, the dynamic stress–strain plot shown in Figure 9 was created.The constitutive parameters extracted from Figure 9 are shown in Table I.

5. EXPERIMENTAL VERIFICATION

In order to compare the analytical predictions with the experimental results, the authors discretized the 10 cm thick peat layer used in the experiment into 10 elements of equal thickness.

The steel bottom of the container was assumed to be infinitely stiff. Hence, the displacement and the velocity of the 10th element were set to zero. In addition, the outer radius of zone 2 was assumed to be $2 \times r_0$ (8·56 cm) where r_0 is the radius of the soil column (zone 1) (Table I). In order to scrutinize the sensitivity of the selected number of elements and the radius of zone 2 on the analysis, variation of the final penetration with the above parameters were plotted as shown in Figures 10 and 11. It is seen that the values of the above parameters can be determined based on Figures 10 and 11 so that a computationally efficient analysis could be performed.

Figure 11 shows that the hammer penetration responds significantly to the change of the radii ratio (zone 2 to zone 1) up to a value of 3·5. It also shows that under the present impact conditions, introduction of the non-linear zone changes the final penetration by only a factor of 0·97. This is mainly due to the fact that during the small-scale laboratory impact considered here, the *in situ* shear strength of the elements in zone 1 is inadequate to enforce the formation of a non-linear zone that provides a transition between the participating soil mass (zone 1) and the stationary zone 3. In case of field dynamic compaction where the influence zone extends to deeper layers with higher lateral stresses, the presence of the non-linear zone will be more significant. Hence Figure 11 by no means indicates an insignificant role of the non-linear transition zone.

In a trial run of the numerical algorithm with $\beta_1 = 0{\cdot}5$, it was found that the results were insensitive to the selected time interval, at time intervals smaller than 0·00005 s for the parameters indicated in Table I. The corresponding analytical prediction of the stress history is plotted against the experimental results in Figure 12, where the agreement between them with respect to the magnitude and time seems to be reasonable.

Furthermore, the penetration predicted from the ultimate value of d_1 was 12 mm while experimentally it was observed to be 7 mm.

Figures 12 and 8 show the eventual introduction of tension at the bottom of the weight mainly due to the suction created by pore water. Although the current analytical technique can predict tensile stresses, due to its inability to incorporate the pore pressure behaviour and tensile soil

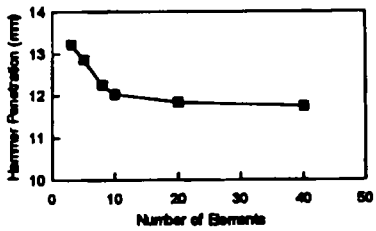

Figure 10. Variation of penetration with element thickness

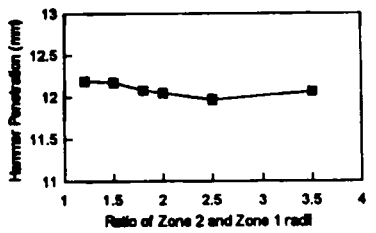

Figure 11. Variation of penetration with the ratio of zone 2 to zone 1 radii

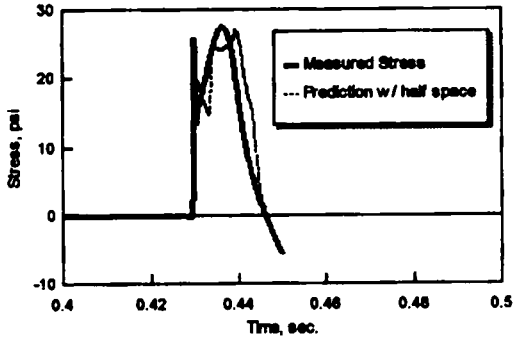

Figure 12. Comparison of measured and predicted stress pulses

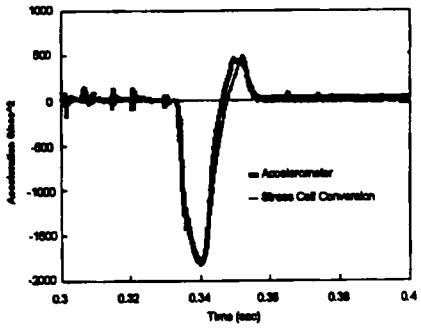

Figure 13. Comparison of the accelerometer and converted stress cell readings

properties, the predicted stress pulse was truncated after the compression wave. It is apparent that a major portion of the penetration descrepancy could be attributed to the rebound of soil during the tension stress pulse.

The authors further verified the accuracy of the measured stresses by comparing the accelerometer reading with the converted average stress cell readings according to the following equation, for another trial impact in the same experimental set-up.

$$a = \frac{[-\sigma_{avg}A + mg]}{m}$$

where

A = base area of the drop weight,
a = acceleration,
m = mass of drop weight,
σ_{avg} = average of stress cell readings.

Figure 13 shows excellent agreement between the accelerometer and converted stress cell readings verifying the accuracy of the above measurements.

6. GUIDELINES FOR USE OF THE MODEL

Reliability of any analytical model depends upon appropriate mathematical idealization of a given engineering problem and accurate determination of the model parameters. Estimation of the zone of influence, element thickness and the radius of the inner zone are the main tasks in the idealization phase of this specific problem. On the other hand, the parameters needed for this specific model are those associated with the constitutive relationship. As previously mentioned, the $\sqrt{(Wh)}$ criterion can be used to estimate the zone of influence while the thickness of individual elements should be decided after a sensitivity analysis using different trial element thicknesses. The outer radius of the non-linear shear zone (zone 1) is usually considered as a multiple of the inner soil column radius and should be based on past experience of the extent of deformation around the hammer. Moreover, in the case of a rectangular or a square hammer, the use of an equivalent radius is advocated.

The parameters needed for the constitutive relationship include initial constrained modulus (M_0), asymptotic strain (ε_0) and the material dependent constant (η). The constrained modulus (M) and the shear modulus (G) are related to the Young's modulus (E) and the Poisson's ratio (ν) by the following expressions:

$$M = \frac{E(1-\nu)}{(1-2\nu)(1+\nu)}$$

$$G = \frac{M(1-2\nu)}{2(1-\nu)}$$

Phillips and Baladi[12] and Nelson[13] suggested that, for loose granular soil, η takes values between 0·80 and 0·90 while ε_0 is between 0·40 and 0·50 for ideal one-dimensional dynamic compression. On the other hand, in loose soils like peat, the authors observed that ε_0 goes up to 1.25 and η takes the value of 0·06 under simulated dynamic compaction. Thus, especially for soft soils, it is advisable to find the parameters using laboratory tests where soils are subjected to similar conditions as that of dynamic compaction. The yield point (σ_b) in the stress–strain curve can be found from the standard bearing capacity equations.

CONCLUSIONS

The stress history of impact loading of soft soils has been studied using analytical and experimental techniques. When the falling weight was instrumented with pressure transducers and an accelerometer, two distinct stress peaks were consistently observed during the dynamic compaction of soft materials like organic soils. Furthermore, as one would anticipate, these impact produce relatively large strains during dynamic compaction leading to permanent deformations.

The above observations cannot be explained by any of the currently available analytical models for impact loading since they incorporate linear stiffness and damping properties. In the improved methodology advanced in this work, the stiffness and damping properties of the entire impact vicinity are modelled using spring and dashpot elements which appropriately represent the deformation modes of the individual zones. Moreover, the different degrees of deformation of the distinct zones are also considered in the model by utilizing nonlinear stiffness properties whereever necessary. On the other hand, when the impact is relatively mild, the non-linear zone becomes insignificant, thus appropriately reducing the model to currently available linear models.

Finally, it was displayed that the current technique posseses the capability of predicting the entire surface stress history including the two distinct peak stresses to a reasonable accuracy. In

addition, its ability to predict the approximate permanent penetration is indeed another advantage of the model.

APPENDIX

A.1. Derivation of the stiffness expression[9] of zone 2

The following stress–strain relationship is used for zone 2:

$$\gamma/\gamma_r = \beta/(1-\beta)$$

$$\beta = \tau/\tau_f$$

$$\gamma_r = \tau_f/G_s \text{where}$$

τ_0 = shear stress at the soil column interface,
τ_f = ultimate shear strength,
G_s = initial tangent shear modulus,
τ = shear stress at radius r from the centre of the impact area.

By assuming plane strain conditions, the displacement at soil column surface (w_0) is obtained by direct integration of the angular distortion from the radius of the zone 1 (r_0 to the radius of the zone 2 r_1).

$$w_0 = \int_{r_0}^{r_1} \gamma \, dr$$

$$w_0 = \int_{r_0}^{r_1} \frac{dr}{\dfrac{1}{\beta\gamma_r} - \dfrac{1}{\gamma_r}}$$

But for the equilibrium of zone 2

$$2\pi r_0 \tau_0 \, dx = 2\pi r \tau \, dx$$

By substituting the above condition and simplifying

$$w_0 = \int_{r_0}^{r_1} \frac{dr}{\left\{\dfrac{G_s r}{\tau_0 r_0} - \dfrac{1}{\gamma_r}\right\}}$$

Then by integrating and simplifying the above equation, it can be proved that $k_3 = \tau_0/w_0$

$$k_{s1i} = \frac{2\pi G_s}{\ln\left[\dfrac{(r_1/r_0) - (\tau_0/\tau_f)}{1 - (\tau_0/\tau_f)}\right]}$$

REFERENCES

1. P. Mayne and J. Jones, 'Impact stresses during dynamic compaction, *J. of Geotechnical Engineering, ASCE* **109**, 1342–1346 (October 1983).
2. R. A. Scott and R. W. Pearce, 'Soil compaction by impact', *Geotechnique*, **25**(1), 19–30 (1975).
3. J. H. Qian, 'Dynamic consolidation from practice to theory', *Proc 8th Asian Regional Conf. on Soil Mechanics and Found. Engrg.*, Vol. 2 Japanese Society for Soil Mechanics and Foundation Engineering, 1986, pp. 213–217.

4. J. W. Roesset, E. Kausel, V. Cuellar, J. L. Monte and Valerio, 'Impact of weight falling onto the ground, *J. Geotech. Eng. Div., ASCE*, **120**, 1395–1412 (1994).
5. Y. K. Chow, D. M. Yong, K. Y. Yong, and S. L. Lee, 'Dynamic compaction analysis', *J. Soil Mech. Found. Div. ASCE*, **118**(8), (1992).
6. L. Menard and Y. Broise, 'Theoretical and practical aspects of dynamic consolidation', *Geotechnique*, London, **25**(1), 3–18 (1975).
7. G. A. Leonards, W. A. Cutter and R. D. Holtz, 'Dynamic compaction of granular soil', *J. Geotech. Eng. Div. ASCE*, **106**(1), 35–44 (1980).
8. J. Lysmer and F. E. Ricart, 'Dynamic response of footings to vertical loading", *J. Soil Mech. Found. Div. ASCE* **92**(1), 65–91 (1966).
9. M. H. E. I. Naggar and M. Novak, 'Non-linear model for dynamic axial pile response', *J. Soil Mech. Found. Div. ASCE*, **120**(2), 308–329 (1994).
10. M. Novak, T. Nogami and F. Aboul-Ella, 'Dynamic soil reactions for plane strain case', *J. Eng. Mech. Div. ASCE* **104**, EM4 953–959 (1978).
11. T. Ginsburg, 'Propagation of shock waves in the ground', *J. Soil Mech. Found. Div. ASCE*, **90**(1), 125–163 (1964).
12. B. R. Phillips and G. Y. Baladi, 'Results of two free-field code calculations versus field measurements for the distant plain 1A event', Misc. Paper S-73-2I, U.S. Army Engr. Waterways Experiment Station, Vicksburg, Ms, 1973.
13. I. Nelson, 'Numerical solution of problems involving explosive loading, in '*Proc. Dynamic Methods in Soil and Rock Mechanics, Vol. 2: Plastic and Long Term Effects in Soils*, A. A. Balkema, Rotterdam, The Netherlands, 1977.
14. O. C. Zienkiewicz, '*The Finite Element Method Vol. 2*, McGraw-Hill New York.